Electrochimica Acta 528 (2025) 146332

Contents lists available at ScienceDirect

Electrochimica Acta

journal homepage: www.journals.elsevier.com/electrochimica-acta

Enhancement of oxygen evolution performance of water splitting at high current density by novel electrodeposited NiFe-LDH coatings

Simón G. Quiroz, Santiago Cartagena, Jorge A. Calderón *

Centro de Investigación, Innovación y Desarrollo de Materiales – CIDEMAT, Universidad de Antioquia, Cr. 53 No 61 – 30, Torre 2, Lab. 330, Medellín, Colombia

ARTICLE INFO

Keywords:
NiFe-LDH
Oxygen evolution reaction (OER)
Water splitting
Electrocatalyst
Electrodeposition

ABSTRACT

Efficient water splitting is a key goal in renewable hydrogen production. However, it is a high-demand energy process. Hence, developing highly efficient and inexpensive electrocatalysts is essential to overcoming this challenge. The cell voltage of the electrochemical water splitting is between 1.8 and 2 V, much higher than the theoretical minimum value of 1.23 V, being the oxygen evolution reaction (OER), the most kinetics limiting process, having overpotentials between 210–330 mV at a current density of 30 mA cm^{-2}. This work develops low-cost and scalable electrodes for OER by electrodeposition of NiFe layered double hydroxide (LDH) coatings, with different Ni:Fe ratios in the electrodeposition bath. Coating obtained with Ni:Fe ratio of 15:1 exhibits the best catalytic activity for OER and shows the lowest Tafel slope of 38.5 $mVdec^{-1}$ and the lowest overpotentials of only 206 and 244 in 1 M NaOH at 30 and 100 $mAcm^{-2}$, respectively, which are the most favorable kinetics parameters respect to those found in literature reports. Furthermore, this developed coating material shows excellent electrocatalytic stability for OER after 80 h of operation at a high current density of 400 $mAcm^{-2}$ in an alkaline medium, which is a typical condition for practical operation of electrolyzers. The developed catalytic coating by electrodeposition technique shows high performance and stability, economical and straightforward reproducibility. It also supports conformational coatings on complex three-dimensional and high-surface-area substrates, like nickel foam, making it a highly scalable process.

1. Introduction

Currently, the application of hydrogen as a means of energy storage has attracted the attention of different research institutions and industries globally. This is motivated in part by developments in renewable energy, which have resulted in a surplus of unused wind and photovoltaic energy [1]. The production of hydrogen from water electrolysis is a good option to enable the use of surplus renewable energy. Hydrogen can play a vital role in a zero-emission future, due to its high energy density (140 MJ/kg), which is more than double that of typical fossil fuels (50 MJ/kg). It can be used in many applications as a fuel and is a suitable medium for large-scale energy storage [2]. Nonetheless, for hydrogen to serve in addressing energy and environmental challenges, several problems that remain in obtaining it must be overcome. In the case of alkaline electrolyzers, the most mature form of technology for carrying out the electrolysis of water, one such challenge that has generated significant interest is how to achieve high energy efficiency [3]. The typical cell voltage when carrying out electrochemical water splitting is between 1.8 and 2 V, much higher than the theoretical minimum value of 1.23 V. Therefore, it is necessary to reduce the overpotentials associated with the hydrogen evolution reaction (HER) that takes place at the cathode and the oxygen evolution reaction (OER) that occurs at the anode [4–6].

Therefore, it is crucial to develop materials with high activity for both OER and HER to enhance the performance of alkaline electrolyzers. Although some noble metals, such as platinum, as well as ruthenium and iridium-based oxides, have been shown to serve as electrocatalytic materials that reduce the overpotential that needs to be applied for HER and OER reactions, the high cost of these precious metals limits their practical application [7–10]. Therefore, it is necessary to investigate catalytic systems that require very low content of these platinum group metals or that use other more abundant catalytic materials. These systems need to be low cost, to allow scaling and have high catalytic activity for OER and HER reactions [11]. Developing efficient electrocatalysts of non-noble metals, composed of elements abundant on the earth, is a highly sought-after goal as it would enable the obtaining of cost-competitive hydrogen. However, the anodic half-cell reaction hinders the efficiency of water electrolysis. The overpotentials in

* Corresponding author.
E-mail address: andres.calderon@udea.edu.co (J.A. Calderón).

https://doi.org/10.1016/j.electacta.2025.146332
Received 30 January 2025; Received in revised form 13 April 2025; Accepted 26 April 2025
Available online 27 April 2025

alkaline water electrolysis are typically between 20–200 mV for HER and 220–330 mV for OER at a current density of 10mAcm^{-2} [12–15]. This is because the mechanism of OER is more complex than its counterpart HER. OER involves multiple steps, some of them requiring the transfer of a single electron, which results in slower kinetics and typically demands higher overpotentials compared to the HER [16,17].

Consequently, this work focuses on developing Ni-based catalysts with Fe additions to enhance the kinetics of OER. Fe incorporation in Ni-based electrodes has received considerable attention due to its multiple roles in the catalytic mechanism. Additions of Fe enhances the conductivity of the catalytic film, optimizes bond energy for the adsorption of OER intermediates, suppresses unwanted metal oxidation steps, and facilitates the metal reduction step required for O_2 evolution [18,19]. In the case of nickel oxides, Fe incorporation has been demonstrated to significantly improve electrochemical performance in the OER [20,21]. Landon et al. reported the formation of a $NiO/NiFe_2O_4$ phase at low Fe concentrations, which plays a crucial role in enhancing oxygen evolution activity [22]. The Ni-Fe ratio is a critical factor in catalytic performance, materials containing 60–90 % Ni w/w exhibit optimal activity for OER [23,24]. Beyond composition, the ability of Ni-Fe-based materials to form amorphous structures with high electrochemically active surfaces is essential for achieving superior electrocatalytic activity [25,26]. Similar to Ni-Fe oxides, Ni-Fe hydroxides also demonstrate excellent OER performance and are commonly found in layered structures [27]. Several studies have shown that Ni-Fe-based double-layer hydroxides (NiFe-LDHs) rank among the most active OER electrocatalysts due to their tunable cation ratios, large surface-to-volume ratio, high density of adaptable catalytic sites, and a layered structure that can be modified through anion exchange to facilitate rapid species diffusion [28–31].

While previous studies have primarily explored Ni–Fe electrocatalytic coatings synthesized via traditional chemical routes, limited attention has been given to the scalable electrodeposition of NiFe-LDH catalytic coatings. Electrodeposition technique offers several key advantages for the synthesis of electrocatalytic materials. This technique enables the direct, binder-free growth of catalysts on conductive substrates, resulting in excellent electrical contact and low interfacial resistance [32–36]. This intimate interface promotes efficient electron transfer and maximizes catalyst utilization. A major advantage of electrodeposition is its ability to synthesize a wide range of materials under ambient conditions, unlike many conventional physical or chemical methods that require elevated temperatures, high pressures, complex and large-time processing [37–40]. Additionally, electrodeposition provides precise control over coating thickness, composition, and morphology by tuning parameters such as applied potential, current density, electrolyte composition, and deposition time. It also supports conformal coatings on complex three-dimensional, high-surface-area substrates (e.g., nickel foam, carbon cloth), facilitating the fabrication of self-supported electrodes with enhanced mechanical robustness and long-term catalytic durability [32–36]. Collectively, these attributes make electrodeposition a scalable, cost-effective, and highly versatile strategy for the fabrication of high-performance electrocatalysts.

Considering that OER presents the higher kinetics limitation of the two reactions in alkaline water electrolysis, in this work, low-cost electrodes for OER are developed by novel electrodeposition of NiFe-LDH coatings. The method has the following advantages: 1) uses a scalable process with low energy requirement, compared with other techniques like hydrothermal, which requires the use of heat for several h, and microwave, which needs the use of specialized equipment. 2) Unlike other methods, where Fe is electrodeposited, there is no need to use N or Ar during the process. 3) quick production time of $<$1 h. 4) it is binder-free, as the catalyst is directly formed on the conductive substrate. 5) A high surface area is generated for this method in one step. 6) common and cheap compounds are used during the synthesis. This work analyzes different Ni:Fe ratios in the electrodeposition bath with the aim of optimizing the coating formulation and obtaining one of the most catalytic NiFe-LDH compound with respect to other already reported, and with great stability in high current densities.

2. Experimental

2.1. Materials and reagents

Commercial nickel foam (NF) with dimensions of approximately 1 cm x 1 cm x 0.16 cm were used as the working substrate. Nickel (II) nitrate hexahydrate (Ni $(NO_3)_2 \cdot 6H_2O$ was purchased from Thermo Scientific $\geq$ 98 %. Ferrous (III) nitrate nonahydrate ($Fe(NO_3)_3\ 9H_2O \geq$ 99.0 %, sodium hydroxide (NaOH) 99.0 %, potassium hydroxide (KOH) $\geq$ 85.0 % were purchased from EMSURE® MERCK.

2.2. Preparation of NiFe-LDH/NF

NF was sonicated in 3 M HCl solution for 5 min to remove the NiO_x on the surface. Then, NF was washed using deionized water. The electrodeposition was carried out in a standard three-electrode electrochemical cell containing NF as the working electrode, platinum mesh as the counter electrode and an Ag/AgCl (3 M KCl) as the reference electrode. The electrolyte bath contained $Ni(NO_3)_2\ 6H_2O$ and $Fe(NO_3)_3\ 9H_2O$ as precursors of the nickel and iron. The molar ratio of Ni:Fe in the electrolyte bath varied between (1:1,2:1,3:1,4:1,5:1, 10:1,12:1,15:1 and 20:1) where differences in catalytic activity are found for the OER. The coatings were electrodeposited via potentiostatic deposition at −1 V (vs Ag/AgCl) for 2400 s at room temperature (23 °C) and in an electrolyte bath with a pH value of 2.0.

2.3. Characterization techniques

The structure and morphology of the coated electrodes (NiFe-LDH/NF) were characterized by scanning electron microscopy (SEM) and the chemical element analysis was performed by energy-dispersive X-ray spectroscopy (EDS), using a JEOL-JSM 6490LV device with accelerating voltage of 20 kV. The crystalline structures of the NiFe-LDH/NF electrode were obtained by X-ray diffraction (XRD) with Cu K_α radiation as the X-ray source (λ=1.54059 Å) operated with a source power of 40 kV and 15 mA from a 2θ from 10° to 80° Phase composition was evaluated through Raman spectroscopy, using a Horiba Jobin Yvon (Labram HR) Nikon (BX41) microscope with a CCD detector (Wright 1024 × 256 pixels) with a laser of 625 nm.

2.4. Electrochemical measurements

OER tests were performed in a AUTOLAB PGSTAT302F potentiostat/galvanostat using a standard three-electrode electrochemical cell at room temperature (~23 °C). The as-prepared electrodes were employed as the working electrodes, a graphite rod electrode was used as counter electrode and Hg/HgO as reference electrode. All measurements were performed using NaOH 1 M electrolyte, except for comparative stability which was performed with KOH 1 M.

The OER performance of the obtained NiFe-LDH/NF electrocatalyst were evaluated using linear sweep voltammetry (LSV) in NaOH (1 M) aqueous electrolyte with a scan rate of 1 mVs^{-1} from 0.3 to 1.10 V. Tafel slopes were obtained from potentiodynamic measurements with a scan rate of 80μVs^{-1}. The electrochemical double-layer capacitances (Cdll) were estimated from cyclic voltammetry (CV) measurement in a non-Faradaic region under different scan rates (10, 20, 30, 40, 60, 80, 100 and 120 mV.s^{-1}). The potential window selected, where no faradaic processes were observed, was from 0.015 to 0.115 V vs Hg/HgO, so that the measured currents only considered the charging of the double layer. A linear fitting of the capacitive current (j) vs. scan rate curve was performed to obtain the double layer capacitance, determined as the slope of the line [41,42]. To study the behavior of the electrode-electrolyte interface, electrochemical impedance spectroscopy

(EIS) was performed using a Zhaner IM6E potentiostat at a potential polarization of 0.525 V vs Hg/HgO in a frequency range from 100 KHz to 10 mHz with 10 mV of amplitude perturbance. The stability of the developed electrodes is evaluated by chronopotentiometries at a high current density of $|400|mAcm^{-2}$ for 25 h.

All potentials reported in this work were converted to a reversible hydrogen electrode (RHE) using the following equation. $E_{RHE} = E_{Hg/HgO} + 0.098 + 0.059pH$. The voltage data were corrected by i-R compensation using the following equation $E_c = E_m - IR_S$. The overpotential (η) for OER was obtained as follow: $\eta = E_{RHE} - 1.23\ V$. Where $E_{Hg/HgO}$ is the measured potential corrected, I is the response current of the measurement at the working electrode and Rs was the ohmic resistance of the solution obtained with current interrupt measurements and EIS.

3. Results and discussion

3.1. Structural and elemental characterization

SEM micrographs at different magnifications of the surface morphology of electrodeposited NiFe-LDH/NF are shown in Fig. 1. The formation of sheets that cover a large part of the surface of the nickel foam is observed for the higher Ni:Fe ratios in the electrodeposition bath. In addition, on these sheets, the formation of other species can be observed, associated with Ni-Fe oxyhydroxides, which provide an increased number of catalytic sites, favoring the performance of the material for OER [43–49]. Fig. 1a shows the substrate NF. It is possible to observe that, for the 2:1 ratio shown in Fig. 1b, there is no presence of the characteristic sheets of NiFe-LDH [50,51]. In that case, only a change on the substrate surface is observed, without any presence of the Ni-Fe coating. This is further confirmed by the EDS, which shows only the presence of nickel, as shown in the data in

Table 1. In the case of the 5:1 (Ni:Fe) ratio shown in Fig. 1c, the sheets are present on the surface of the foam, but they do not cover a large amount of the surface of the substrate, which is also shown to be the case for the 4:1 and 3:1 coatings. Those coatings are shown in **Figure S1** in the supplementary material, where it is possible to observe that the coating is not present homogeneously on the entire surface of the substrate. More homogeneous coatings were obtained with the 10:1 and 15:1 ratios (Fig. 1d-e). These were the coatings with the best results, as will be discussed later. In the case of 20:1 ratio, some areas are not totally covered by the deposited material or where the coating begins to detach from the substrate, see Fig. 1f. Therefore, lower performance for the OER is expected in this case. Also, it can be observed that the presence of the NiFe-LDH coating on NF generates a rougher surface as Ni:Fe ratio increases. Therefore, the electroactive surface area of the electrode is also expected to increase.

Table 1
EDS analysis for NiFe coatings.

Sample	Ni (at.%)	Fe(at.%)	O(at.%)
1:1	100	–	–
2:1	100	–	–
3:1	81.06	1.52	17.42
4:1	8.85	19.52	71.63
5:1	14.16	34.62	51.22
10:1	9.67	33.06	57.27
12:1	11.15	23.93	64.92
15:1	9.83	28.07	62.10
20:1	11.14	20.02	68.83

Table 1 shows the results of the EDS elemental analysis. As can be seen, the coatings contain Ni, Fe, and O, as expected for the material. It is confirmed that, for low ratio coatings, there is no presence of elements other than nickel (1:1 and 2:1). In addition,

Table 1 shows that the intermediate Ni:Fe ratios used in the electrolytic bath produce deposits with higher content of Fe than Ni in the coating. This indicates a preference for the deposition of Fe over Ni, even though iron is the less noble metal of the two. This phenomenon, called "anomalous co-deposition", is consistent with literature reports, which describe the preferential deposition of the less noble metal with respect to the more noble one [52–54]. The literature mentions several possible mechanisms that could explain this behavior, but one of the most accepted is that the inhibition of Ni deposition in the presence of Fe is due to the preferential adsorption of intermediate iron species on the electrode surface [55–59].

Fig. 2 shows the X-ray diffraction (XRD) patterns of NiFe-LDH coatings electrodeposited from baths with different Ni:Fe ratios. No diffraction peaks corresponding to the characteristic crystalline phase of NiFe-LDH were observed below of $2\theta = 35°$. However, the characteristic morphology in plates and further Raman spectroscopy analysis (next section) demonstrate the existence of NiFe-LDH compound on the catalytic coating. The XRD result indicates that an amorphous structure of NiFe-LDH is achieved. This observation is consistent with previous

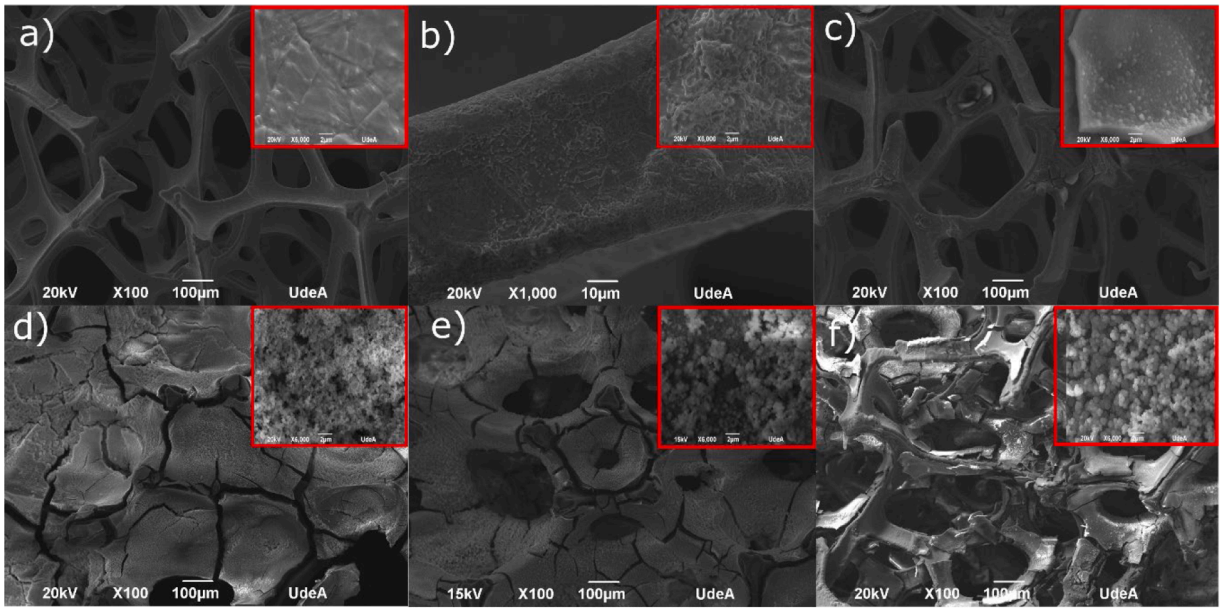

Fig. 1. SEM micrographs for different Ni:Fe ratios at of x100 and x6000 magnifications. a) NF. b) Ni:Fe 2:1. c) Ni:Fe 5:1. d) Ni:Fe 10:1. e) Ni:Fe 15:1. f) Ni:Fe 20:1.

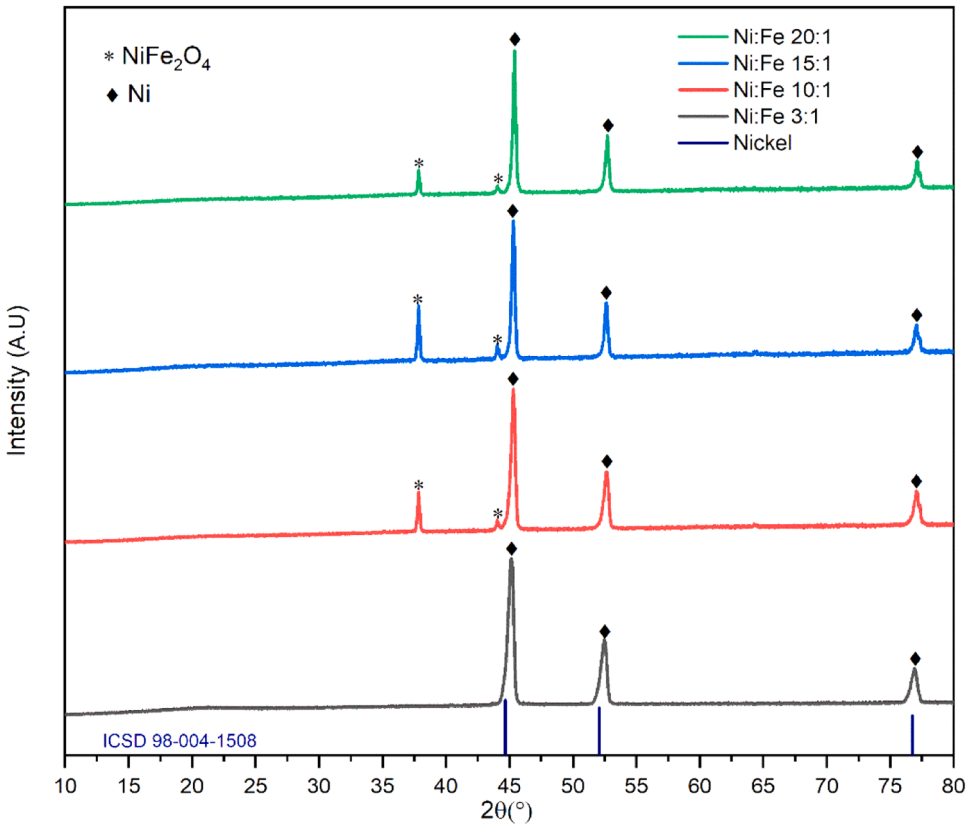

Fig. 2. XRD patterns for different Ni:Fe ratios.

literature reports indicating that NiFe-LDH compounds synthesized by electrodeposition commonly exhibit an amorphous structure [60–62]. Moreover, it has been widely reported that amorphous NiFe-LDHs display superior catalytic activity toward the oxygen evolution reaction (OER) compared to their crystalline counterparts. This enhancement is attributed to lattice distortions at the surface of the amorphous

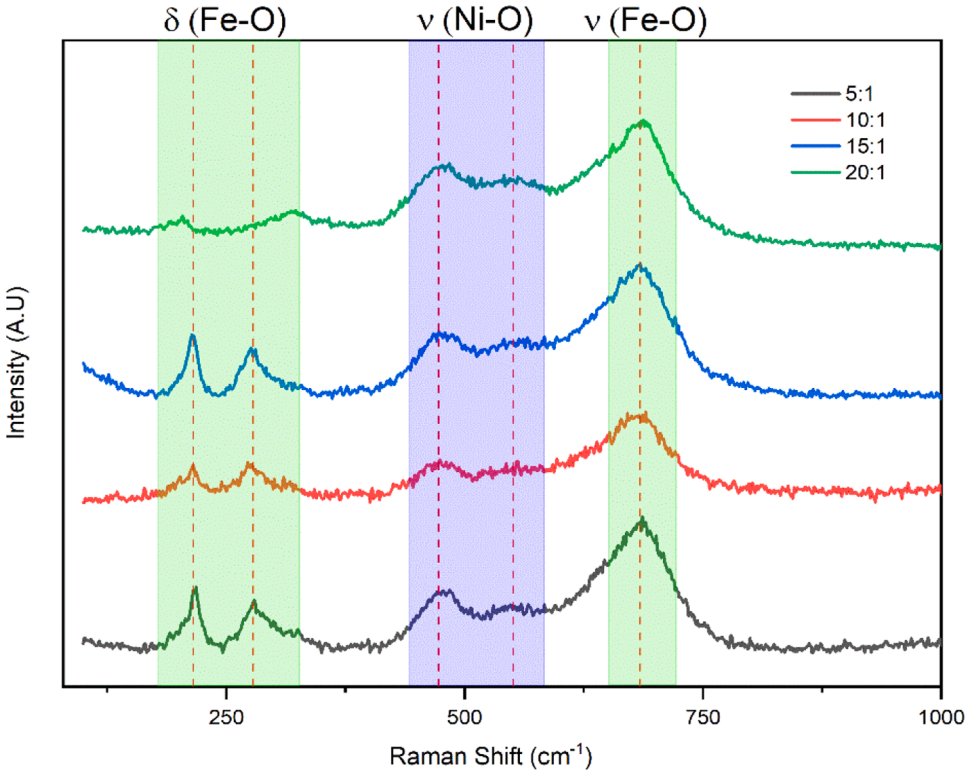

Fig. 3. Raman spectra obtained for the different NiFe-LDH coatings.

metal or metal oxide, which lead to the formation of abundant active sites, thereby resulting in higher OER activity compared to crystalline hydroxides [63–68]. The diffractogram for the ratio of 3:1 shows peaks at 2θ associated exclusively with the substrate (Ni foam) at 45.38°, 52.6°, and 77.05° [27,69]. A similar result is observed for the 5:1, 4:1, 2:1, and 1:1 ratios, as shown in **Figure S2**. In the case of coatings with high Ni: Fe ratios in the bath (10:1, 12:1, 15:1, and 20:1), additional peaks at 37.88° and 44.12° appear, which suggests the presence of the $NiFe_2O_4$ phase [45,70]. The integration of the $NiFe_2O_4$ phase into NiFe-LDH materials significantly enhances the catalytic activity of the surface to the OER reaction, as well as improving mass transport and charge transfer at the electrode [45,71].

Raman spectroscopy measurements were performed to determine the main compounds formed after the electrodeposition of coatings on

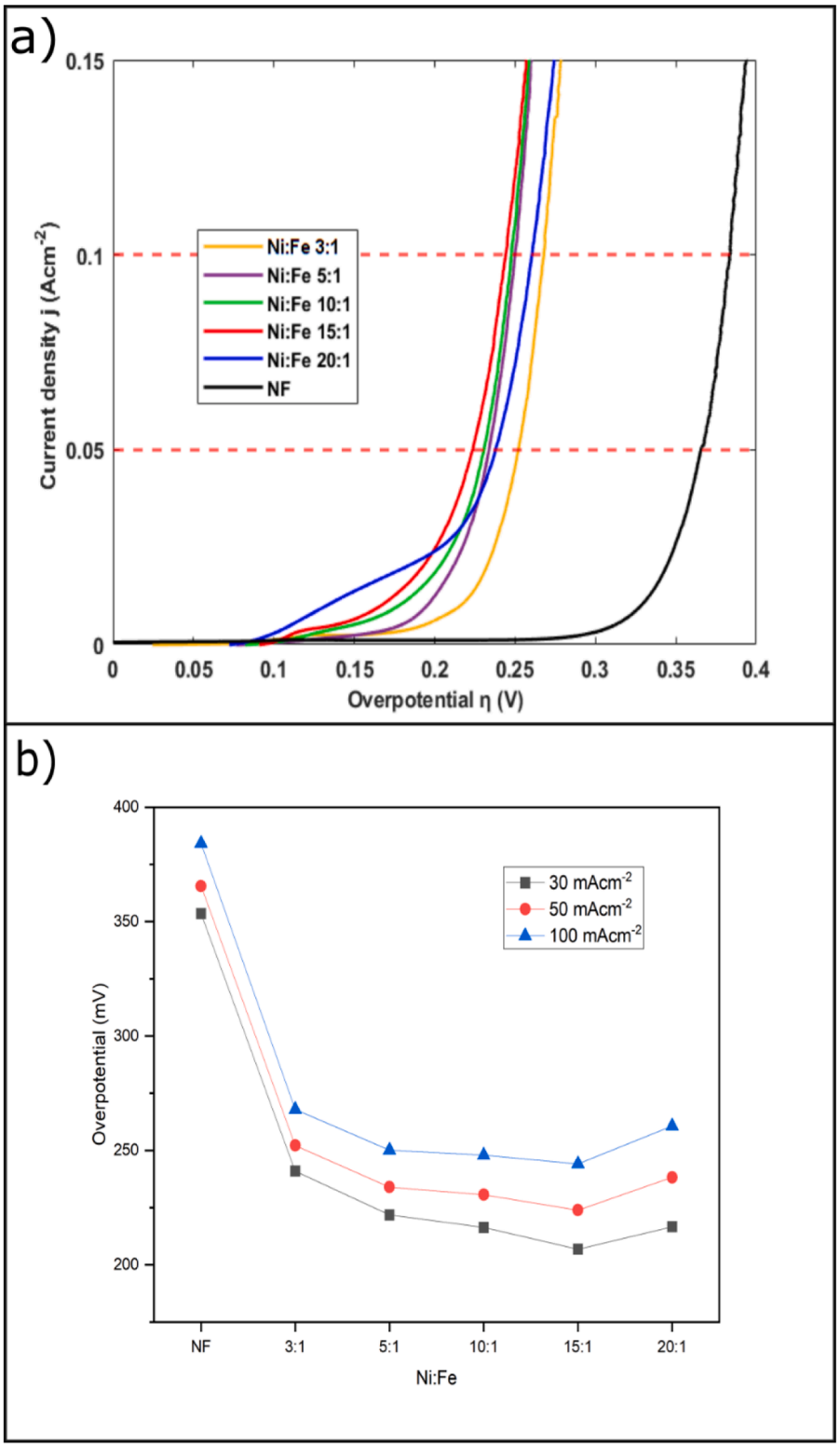

Fig. 4. OER Performance of Ni-Fe samples in 1 M NaOH. a) Anodic evaluation LSV for OER. b) Anodic overpotential obtained for OER (at 30, 50, and 100 $mAcm^{-2}$).

the nickel foam substrate. Fig. 3 shows the Raman spectra of the coatings obtained for different Ni:Fe ratios. Bands observed at 211.1, 279.6, and 684.6 cm^{-1} are associated with the binary oxide $NiFe_2O_4$ [70,72]. This result agrees with the findings obtained with the diffractograms. These vibration modes correspond to the asymmetrical and symmetrical bending of the oxygen atom in the Fe-O bond and the symmetrical stretching of the Fe-O, respectively [71]. The bands located at 472.8 and 552.5 cm^{-1} are attributed to the stretching vibrations of Ni-O of the NiFe-LDH [27,73–76]. Raman spectroscopy technique reveals the formation of NiFe-LDH compound during the electrodeposition of the coating.

3.2. OER test performance

The OER performance of the developed electrocatalytic coatings was evaluated in an alkaline medium (1 M NaOH) through linear sweep voltammetry, as shown in Fig. 4a. The effect of varying the Ni:Fe ratio in the electrodeposition bath on the catalytic performance of the coatings for the OER is evident by the leftward displacement of the curves. The results indicate that, as the Ni:Fe ratio increases, there is a decrease in the overpotential of OER, resulting in a higher current density with a lower overpotential applied to the electrode for the OER reaction. These results confirmed the benefit of Fe addition on catalytic performance of the Ni coatings.

Fig. 4b shows the overpotential behavior as the Ni:Fe ratio varies, revealing a minimum value at a ratio of 15:1. This trend is replicated for different current densities (30, 50, and 100 $mAcm^{-2}$). It can be observed that, beyond the 15:1 ratio, the overpotential required for the OER increases once again. The electrocatalytic material exhibiting the best performance is the one obtained with an Ni:Fe ratio of 15:1, achieving overpotentials of 206.86, 223.89, and 244.13 mV for current densities of 30, 50, and 100 $mAcm^{-2}$, respectively. In contrast, for the uncoated substrate, overpotentials of 353.28, 365.53, and 384.24 mV are observed at current densities of 30, 50, and 100 $mAcm^{-2}$. These values are significantly higher than those obtained with any of the electrodes evaluated with the NiFe-LDH coatings, demonstrating that the developed material coating enhances the catalytic activity of the electrode in the OER.

Table 2 compares the performance of similar NiFe-LDH catalytic materials reported in the literature with the current coating material developed by the electrodeposition method in this work. The literature reports indicate several different methods of synthesis of the NiFe-LDH compound, such as hydrothermal, PLAL (pulsed laser ablation in liquid), solvothermal, and microwave. While sol-gel synthesis involves multiple stages, including gelation, drying, and thermal treatments that can take several hours to days and require high temperatures, leading to high energy consumption, and typically necessitates the use of binders to adhere the material to the substrate, introducing additional ohmic resistance [39,77,78]. Hydrothermal synthesis also requires long reaction times under elevated temperature and pressure conditions, often necessitating the use of autoclaves and, in some cases, post-synthesis thermal treatments [37,38,79]. In contrast, electrodeposition is performed under ambient temperature and pressure conditions, simplifying the process, reducing energy demands, and improving safety. It enables direct, in situ synthesis of catalytic materials on conductive substrates without binders, improving mechanical adhesion and reducing interfacial resistance, thus enhancing charge transfer efficiency and catalyst utilization. Additionally, electrodeposition allows precise control over key parameters such as composition, thickness, and morphology of the coating by adjusting applied potential, current density, electrolyte composition, and deposition time [32–36]. The process is also notably faster, taking only a few minutes compared to the several hours required by sol-gel or hydrothermal methods. These features make electrodeposition a versatile, scalable, and cost-effective technique for fabricating high-performance, self-supported electrodes. Table 2 shows that the catalytic performance in OER of the material developed in this work is better than that of other NiFe-LDH developed. The NiFe-LDH material with the best performance of those developed (Ni: Fe 15:1) exhibits excellent OER activity with low overpotentials compared to other NiFe-LDH materials at different current densities (30, 50, and 100 $mAcm^{-2}$). Additionally, the NiFe-LDH material (15:1) shows lower overpotentials than NiFe-LDH materials doped with Zn or Co, as well as other modified materials such as sulfated NiFe-LDH and RuO_2/NiFe-LDH/NF.

3.3. Kinetics study of OER

Fig. 5 shows the Tafel slopes of the NiFe-LDH coating material, used to study the kinetics of the OER. Two Tafel slopes were observed, one for low overpotentials and the other for high overpotentials. The presence

Table 2
Comparison of the OER performance of various NiFe -based electrocatalysts reported in literature and in this work.

Material	Method Syntesis	Electrolyte	Overpotential (mV)	Current density ($mAcm^{-2}$)	Reference
Ni_6Fe_4LDH	grinding	1 M KOH	280	10	[80]
NiFe@LDH	Hydrothermal	1 M KOH	260	10	[40]
v-l-LDH/NF	drip method	1 M KOH	230	100	[81]
NiFe-LDH@NF	Hydrothermal	1 M KOH	210	10	[82]
Ni_2Fe_1-LDH	Hydrothermal	1 M KOH	245	10	[83]
Ni_2Fe_1-LDH	Hydrothermal	1 M KOH	295	30	[83]
Zn-NiFe-LDH	Hydrothermal	1 M KOH	218	10	[84]
$Co_{1.98}$—NiFe LDH	Solvothermal	1 M KOH	266	50	[85]
$Co_{1.98}$—NiFe LDH	Solvothermal	1 M KOH	290	100	[85]
NiFe-LDH	Hydrothermal	1 M KOH	270	80	[86]
Ni/Fe_3O_4 / NiFe LDH	Hydrothermal	1 M KOH	275	20	[87]
NiO/NiFe LDH	PLAL*	1 M KOH	205	30	[43]
NiFeZn LDH	Hydrothermal	1 M KOH	204	10	[88]
NiFeZn LDH/NF	Hydrothermal	1 M KOH	323	100	[89]
Sulfated NiFe LDH	Microwave	1 M KOH	288	50	[90]
Sulfated NiFe LDH	Microwave	1 M KOH	339	100	[90]
RuO_2/NiFe-LDH/NF	Hydrothermal	1 M KOH	226	10	[91]
RuO_2/NiFe-LDH/NF	Hydrothermal	1 M KOH	319	50	[91]
PR-NiFe-LDH	Hydrothermal	1 M KOH	278	10	[92]
NiFe-LDH/CNTs	Hydrothermal	1 M KOH	269	20	[93]
NiFe-LDH 15:1	Electrodeposition	1 M NaOH	**206**	30	This Work
NiFe-LDH 15:1	Electrodeposition	1 M NaOH	**223**	50	This Work
NiFe-LDH 15:1	Electrodeposition	1 M NaOH	**244**	100	This Work

* PLAL(Pulsed Laser Ablation in Liquid).

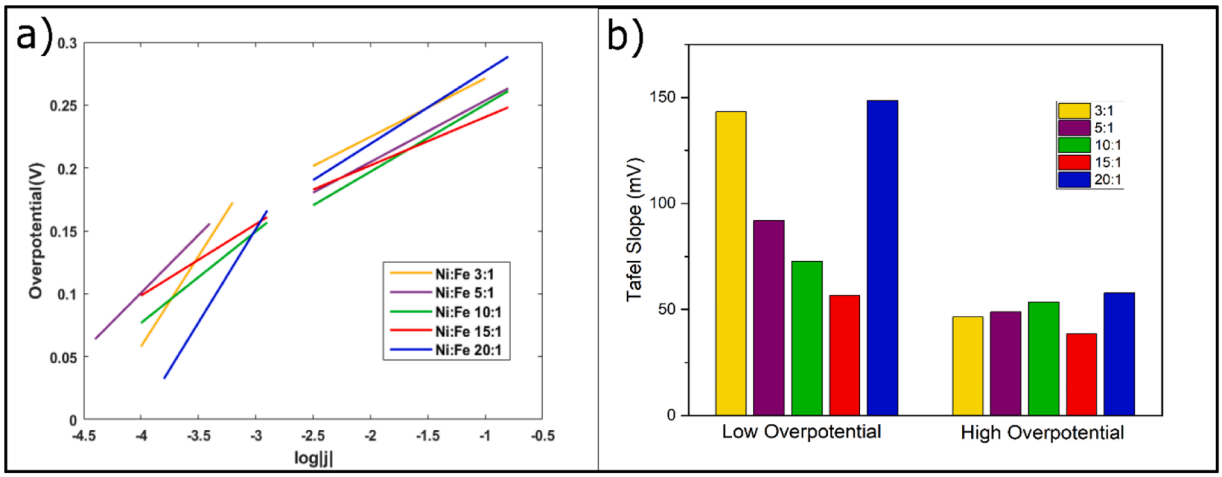

Fig. 5. Tafel plots of the OER of NiFe-LDH/NF electrocatalytic coating in 1 M NaOH. a) OER Tafel plots for NiFe-LDH/NF. b) Variation of Tafel slopes to low and high overpotentials.

of two slopes in the polarization curves suggests that it is likely that two different electrochemical processes are occurring due to the formation of different species and kinetics steps that limit the reaction during anodic polarization at low and high overpotentials [94,95].

Table 3 summarizes the Tafel slope values for NiFe-LDH coating materials. Notably, a Ni:Fe ratio of 15:1 yields the lowest Tafel slopes, of 56.7 mVdec^{-1} and 38.5 mV dec^{-1} for low and high overpotentials, respectively. It is important to highlight that the lowest Tafel slope value of 38.5 mV dec^{-1} is obtained at high polarization, which is the most common condition in which electrolyzers are operated. This indicates favorable kinetics conditions for the performance of water electrolysis at high current densities and high polarization. Comparing these Tafel slope values with those reported in the literature for NiFe-LDH, which typically range between 40–50 mVdec^{-1}, it can be stated that the developed material with an Ni:Fe ratio of 15:1 exhibits significant catalytic activity, better than that previously reported for OER [71,90,96,97].

The general mechanism of the OER reaction in an alkaline environment is typically described by Eqs. (1)–4, with the corresponding and indicated Tafel slopes [98–100].

$$M + OH^- \leftrightarrow MOH + e^-,\ b = 120\ mVdec^{-1} \quad (1)$$

$$MOH + OH^- \leftrightarrow MO^- + H_2O,\ b = 60\ mVdec^{-1} \quad (2)$$

$$MO^- \rightarrow MO + e^-,\ b = 45\ mVdec^{-1} \quad (3)$$

$$2MO \rightarrow 2M + O_2,\ b = 19\ mVdec^{-1} \quad (4)$$

Each of these reactions has an associated Tafel slope, providing insights into the limiting step of the OER reaction. In the case of the Ni-Fe 15:1 material, which demonstrated the best performance of the developed electrocatalytic materials, a slope close to 60 mVdec^{-1} is observed for low overpotentials. This suggests that the rate-determining step (RDS) at low overpotentials is associated with reaction (2), specifically related to the adsorption of an intermediate species during the OER. Conversely, at elevated overpotentials where Tafel slopes below 60 mV dec^{-1} are recorded, the reduction in the Tafel slope indicates a shift in the rate-determining step (RDS) toward reaction (3), suggesting that the electrochemical oxidation of adsorbed MO^- intermediates become the dominant pathway.

Table 3
Tafel Slopes for low and high overpotentials.

Tafel Slope Low Overpotential		Tafel Slope High Overpotential	
Sample	Slope(mVdec^{-1})	Sample	Slope (mVdec^{-1})
3:1	143.3	3:1	46.4
5:1	91.9	5:1	48.8
10:1	72.7	10:1	53.4
15:1	**56.7**	**15:1**	**38.5**
20:1	148.6	20:1	57.7

Commonly, a higher electrochemically active surface area (ECSA) is associated with more active sites at the solid-liquid interface [83]. A direct evaluation of the relative ECSA of electrocatalysts by cyclic voltammetry (CV) can be done by estimating the electrochemical double layer capacitance (Cdl) [101]. To obtain the electrochemical double layer capacitance for the electrodes developed with the NiFe-LDH coating, the procedure already mentioned in the experimental methodology is followed. Here, different cyclic voltammetry measurements were performed at the non-faradaic region with scanning rates between 10 – 120 mVs^{-1}. It should be clarified that this procedure was only followed for samples where the presence of the electrocatalytic material was shown. The CV plots of the evaluated materials are shown in **Figure S3** in the supplementary material. The results obtained for the double-layer capacitance using this method are shown in Fig. 6.

To determine the electrochemical active surface area (ECSA), the slopes obtained by plotting the capacitive current against the scan rate (Fig. 6) were used. This slope represents the electrochemical double layer capacitance (*Cdl*). The *ECSA* values were calculated using the *ECSA* = *Cdl/Cs* relationship, where *Cs* is the specific capacitance [102]. *Cs* represents the capacitance of an electrode with a flat surface of the electrocatalytic material. For Ni-Fe materials, *Cs* conventionally has an average value of 40 μFcm^{-2} in an alkaline media [42,69,102,103]. Values of *ECSA* for NiFe-LDH coating materials were calculated as 7.35, 9.12, 8.91, 10.58, and 10.01 cm^2 for coatings with Ni:Fe ratios of 3:1, 5:1, 10:1, 15:1, and 20:1, respectively. Considering the results obtained, the highest *ECSA* value was that exhibited by the electrocatalytic coating with Ni:Fe ratio equal to 15:1. This coating material also exhibited the best performance for OER and the lowest Tafel slopes. However, the values of ECSA obtained in the current work are lower than those found in other works, where ECSA values between 50 – 500 cm^2 have been reported [91,96,104,105]. For this reason, we believe that the outstanding performance of the developed catalytic NiFe-LDH coatings is due to the improvement of the catalytic activity of the material, as indicated by its low anodic overpotentials and low Tafel slopes.

To study the phenomena that occur at the electrode/electrolyte interface and to gain information about the kinetics of charge transfer during the OER on electrocatalytic coatings, electrochemical impedance spectroscopy (EIS) tests were performed for NiFe-LDH systems developed with Ni:Fe ratios of 10:1, 12:1, 15:1 and 20:1. The Nyquist

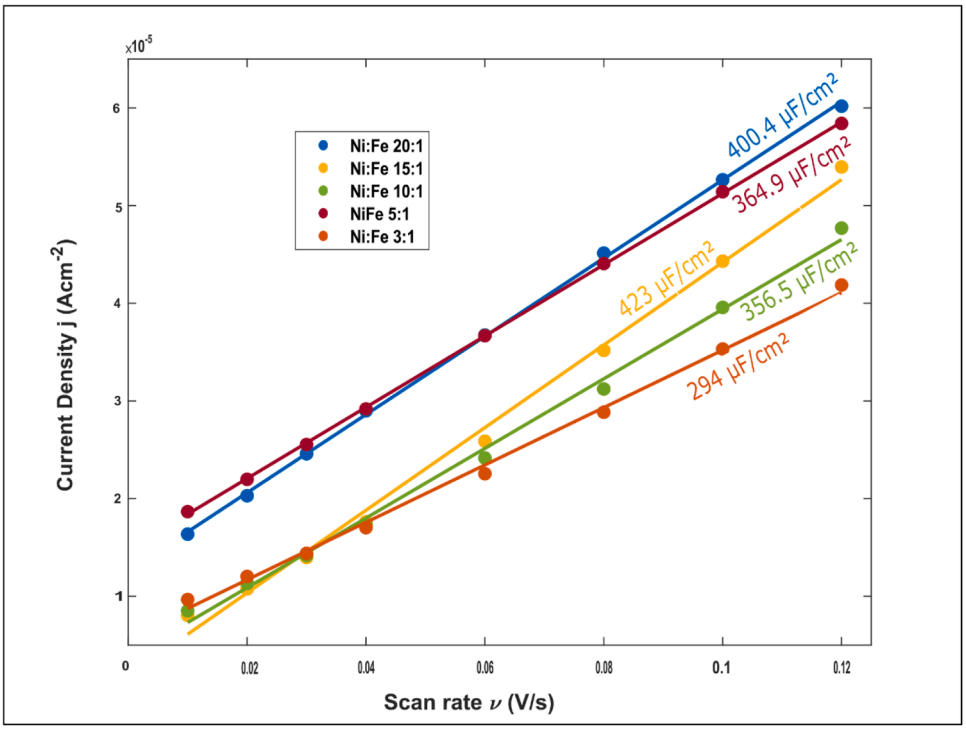

Fig. 6. Capacitive current density vs. scan rate plot to obtain double-layer capacitance for NiFe-LDH/NF materials.

diagrams are represented by the equivalent electrical circuit shown in Fig. 7 where R_s is the ohmic resistance, R_t is the charge transfer across the electrode/electrolyte interface and CPE_{dl} is the constant phase element that represents the double-layer capacitance. R_a and CPE_a are the resistance and constant phase element related to adsorption limitations, desorption, and mass transfer of the adsorbed species on the working electrode [94,106,107]. Fig. 7 shows the Nyquist diagrams of EIS for the different NiFe-LDH coating materials evaluated at anodic potential of 0.525 V vs Hg/HgO (180 mV of overpotential). This anodic polarization potential was chosen to carry out EIS measurements because no oxide transformation reaction occurs in an appreciable form at this potential, and the most important anodic reaction that takes place is the OER, as can be seen in the LSV curves already shown in Fig. 4a.

The values of the electrical parameters extracted from the fit of EIS

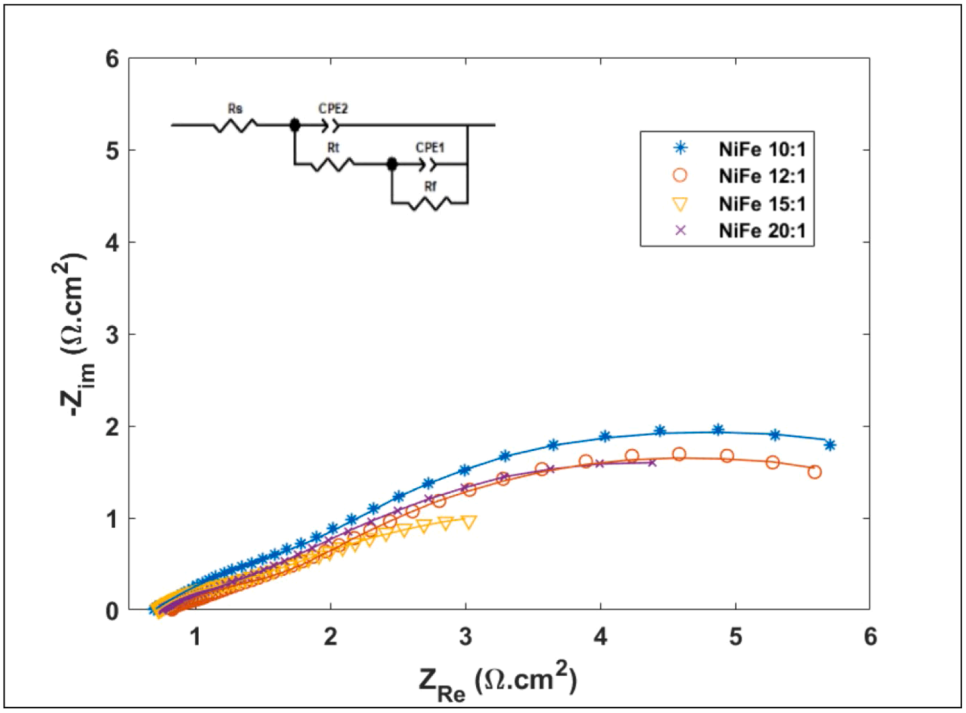

Fig. 7. Nyquist diagrams of EIS measurement for Ni-Fe coatings performed at an anodic potential of 0.525 V vs Hg/HgO. Dots are experimental measurements; lines are fit data with the equivalent electrical circuit (inset).

measurements with the equivalent electrical circuit model are presented in Table 4. The coating with Ni:Fe ratio of 15:1 exhibits the lowest charge transfer resistance, so the rate at which charge transfer occurs for OER is expected to be faster [96]. This coating exhibits higher catalytic activity than the other coatings developed. This is consistent with the results obtained in the different electrochemical tests performed. In addition, the effective double-layer capacitance estimated by EIS for the NiFe 15:1 material is the highest of all the coatings, which is consistent with that obtained by the cyclic voltammetry method.

3.4. OER stability test

The stability of the coating materials developed for OER was evaluated by chronopotentiometry under operating conditions of a conventional electrolyzer, applying an anodic current density of |400| $mAcm^{-2}$ for 25 h. Potentiometric curves of the electrocatalytic coatings are shown in Fig. 8. The material that presented the best performance in the stability test for 25 h was the electrode prepared with a Ni:Fe ratio of 15:1. The overpotential of that electrode stayed between 300–320 mV throughout the test. This electrocatalytic coating also showed the best results in the anodic evaluation by LSV, the lowest Tafel slope of the materials evaluated, and the highest catalytic surface according to the ECSA results. All these results agree with what was obtained in the stability test. In general, the results of the coating materials (10:1, 12:1, and 15:1) show that, after 5 h of high current density application, a stable value is reached over time because the overpotential varies only between approximately 10 – 20 mV during the following 20 hours. However, for the catalytic coating prepared with an NiFe ratio of 20:1 there is a greater increase in overpotential during the test, reaching up to 350 mV at the end of the test. This is because there are areas that are not totally covered by the deposited material, or where the coating begins to detach from the substrate, causing it to have a lower performance for OER.

It is important to highlight that all the electrocatalytic coatings showed better performance for OER after anodic polarization (|400| $mAcm^{-2}$) for 25 h. This was evidenced by comparing the LSV curves performed at 0 h and after 25 h of polarization, as shown in **Figure S4.** It can be seen that after 25 h of polarization at high anodic current density, there is a reduction of approximately 10 mV in the anodic overpotential during OER for all prepared electrocatalytic coatings. This result is associated with the morphological and structural changes of the surface of the coating due to anodic polarization, since additional catalytic species can be formed [47–49]. This was confirmed by SEM analysis performed on the samples after chronopotentiometry measurements, see **Figure S5** in the supporting information. It can be observed that there is a change in the surface morphology of the coating, which can be associated with the appearance of Ni-Fe oxyhydroxide species formed during polarization [27,108,109]. This was further confirmed by the Raman spectra of the electroactive coating (Ni:Fe ratio of 15:1) taken after 80 h of anodic polarization at 400 $mAcm^{-2}$, see Fig. 9. Raman spectra show two bands at 467 and 544 cm^{-1}, corresponding to the formation of nickel oxyhydroxides [73,110,111]. These results demonstrate the formation of a stable catalytic phase of nickel oxyhydroxides, which explains the good electrochemical performance of the coating material, even after 80 h of continuous high polarization in an alkaline environment.

Table 4
Results obtained from the equivalent circuit for the adjustment of the Nyquist diagram for the different ratios.

Sample	*Rs* ($\Omega.cm^2$)	*Rt* (Ω.cm2)	*Ra* ($\Omega.cm^2$)	*Ca* ($mF.cm^{-2}$)	*Cdl* ($mF.cm^{-2}$)
10:1	0.68	3.640	4.75	33.395	406.761
12:1	0.74	1.918	6.99	38.946	343.882
15:1	0.72	0.975	4.22	53.212	1528.564
20:1	0.74	2.036	6.50	40.371	387.566

The elemental surface chemical composition of the materials after the stability test was obtained by EDS analysis, shown in **Table S1** in the supporting information. The coatings are mainly composed of Ni, Fe, and O. The corresponding EDS spectra are shown in **Figure S6,** next to the SEM image of the corresponding area where the information is obtained. Based on the results presented, the long-term stability of the electrocatalytic coatings is primarily attributed to an activation process driven by electrochemically induced surface restructuring, rather than to passivation caused by Fe leaching. After 25 h of anodic polarization at a high current density (400 mA cm^{-2}), all coatings exhibited an improvement in electrocatalytic activity, evidenced by a reduction of approximately 10 mV in the overpotential observed in the LSV curves. This behavior indicates a progressive enhancement of the active surface, which is characteristic of activation processes. Furthermore, post-electrochemical SEM analysis revealed significant morphological changes on the coating surfaces, consistent with surface restructuring. This transformation was associated with the formation of Ni–Fe oxyhydroxide species, as confirmed by Raman spectra showing characteristic bands at 467 and 544 cm^{-1}, corresponding to catalytically active NiOOH phases. The presence of these active phases, along with the coating's ability to maintain high performance even after 80 h of continuous operation, suggests that a stable catalytic phase formed during anodic polarization. This rules out a passivation mechanism linked to Fe leaching, which would typically be associated with a progressive decline in catalytic activity.

The electrolyte change affects the performance of the electrode and the overall electrolysis reaction [15]. For alkaline water electrolysis, the most used electrolyte is a potassium hydroxide solution with a typical concentration between 20–30 wt% due to its high specific conductivity under the typical operating conditions of an alkaline electrolyzer [112]. However, a cheaper alternative is sodium hydroxide, an electrolyte with a lower specific conductivity than KOH [113]. A long-term stability test was then performed for the catalytic coating that showed the best performance (Ni:Fe 15:1), comparing the electrolyte change from 1 M NaOH to 1 M KOH. The results of this test are shown in Fig. 10, where it is possible to observe the effect of the conductivity of the electrolyte on the overpotential value. A more conductive electrolyte is expected to facilitate the mobility of charged species to the electrode/electrolyte interface, thus improving the OER. In addition, other studies mention that there is a direct influence of alkali metal cations on the OER, concluding that larger cations with lower hydration energy can generate greater access of the reactants to the active sites, improving the kinetics of the OER by favorably altering the adsorption energy and improving the rate of formation of key intermediates of the reaction [114–117]. When using 1 M KOH as the electrolyte, the NiFe electrode can achieve a lower overpotential compared to 1 M NaOH electrolyte at 400 $mAcm^{-2}$. The electrode in the 1 M KOH electrolyte produced overpotentials ranging from 250–270 mV, while the electrode in the 1 M NaOH electrolyte yielded overpotentials ranging from 300–320 mV. Therefore, there is a difference in overpotential of around 50 mV between the two electrolytes. In addition, when the electrodes are evaluated by LSV before and after polarization at high current density for 80 hours in each electrolyte, there is no evidence of loss of catalytic activity of the coatings, and the electrochemical performance for OER is similarly preserved in both electrolytes, as shown in **Figure S7** in the supporting information.

4. Conclusions

In this work NiFe-LDH electrocatalysts were obtained on nickel foam by means of a simple electrodeposition method, varying the ratio between nickel and iron present in the bath. The best performing Ni-Fe coating material developed was obtained with a 15:1 ratio in the bath. This catalytic coating showed overpotentials of only 206, 223 and 244 mV for OER, for current densities of 30, 50 and 100 $mAcm^{-2}$, respectively, which is a significantly better performance compared to similar

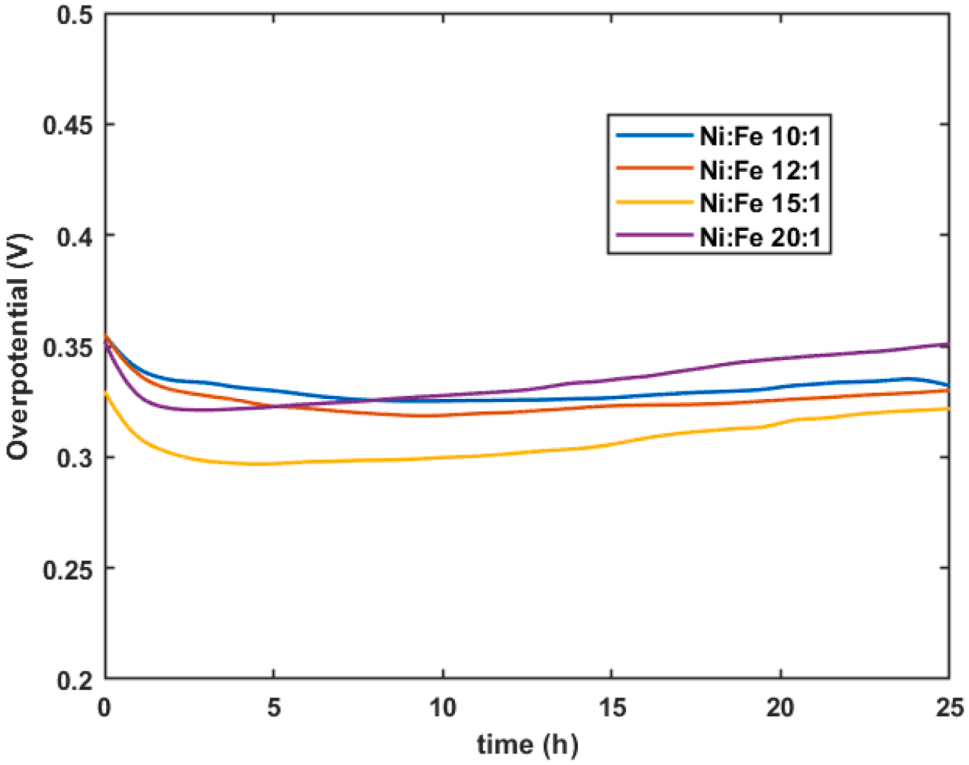

Fig. 8. Chronopotentiometry of NiFe-LDH/NF materials at |400| $mAcm^{-2}$ in 1 M NaOH.

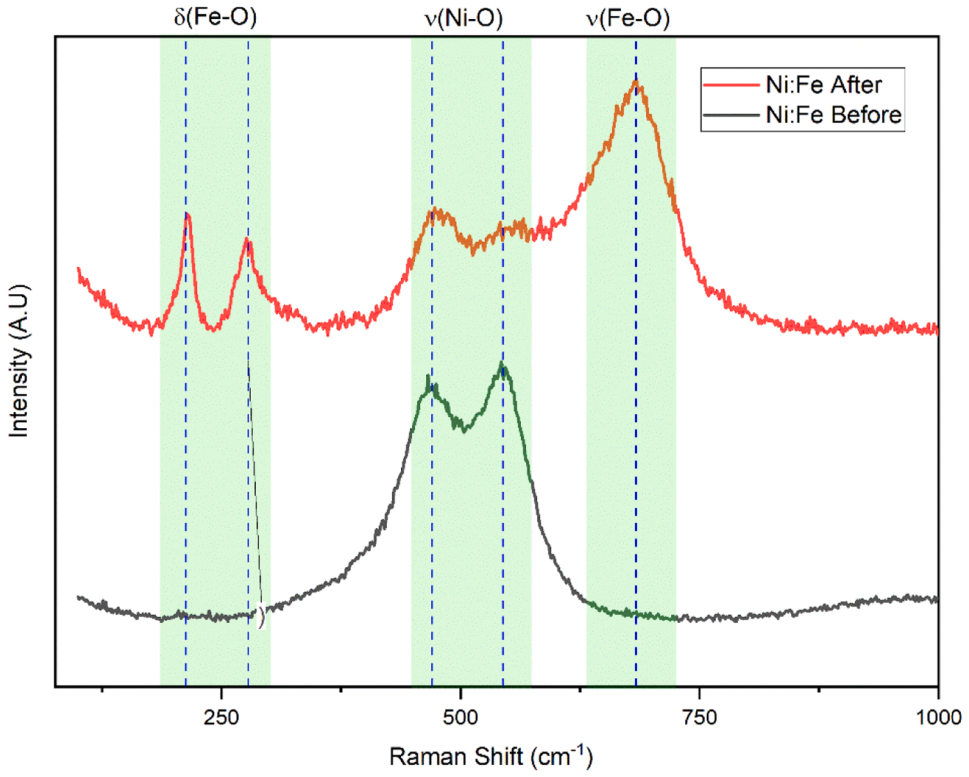

Fig. 9. Raman spectra of electroactive coating (Ni:Fe 15:1) obtained after 80 h of anodic polarization at 400 $mAcm^{-2}$.

catalytic materials reported in the literature. This material showed low Tafel slopes of 56.7 $mVdec^{-1}$ and 38.5 $mVdec^{-1}$ for low and high anodic polarizations, the ECSA was 10.58 which is lower than other materials reported in the literature, so the high catalytic activity is result of the intrinsic activity of the material and not for the surface area. In addition, the stability test at high current density of |400| $mAcm^{-2}$ for 80 hours in 1 M NaOH and 1 M KOH revealed that the coating material maintains excellent catalytic activity and stability in alkaline environments. These

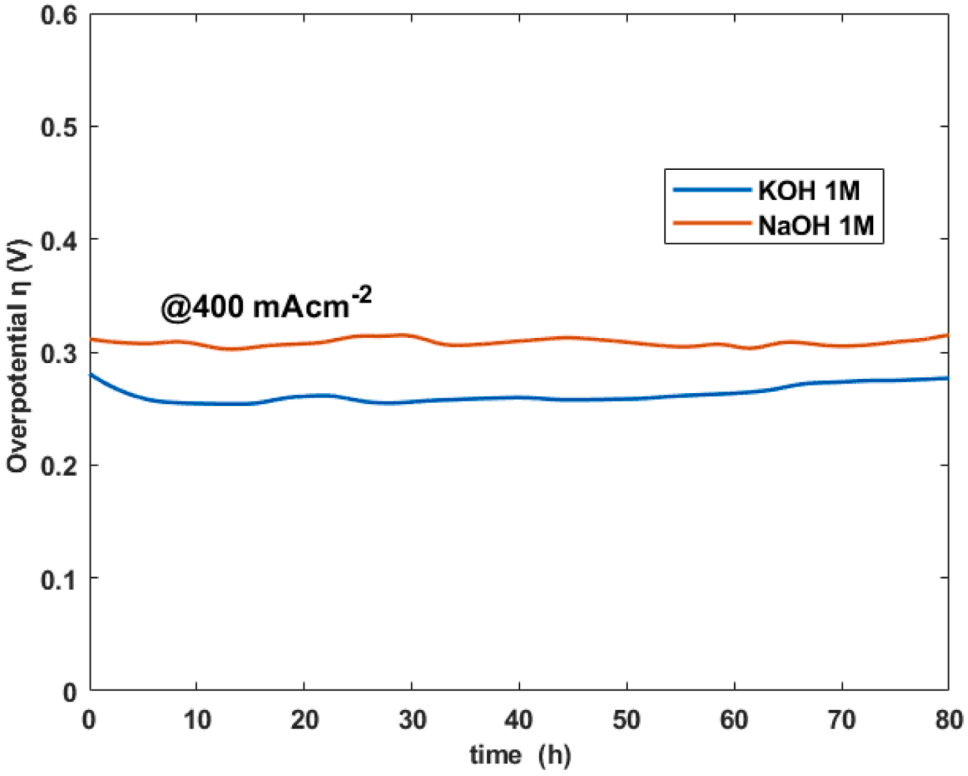

Fig. 10. Anodic stability at 400 mAcm^{-2} for 80 hours for the Ni:Fe 15:1 material in 1 M NaOH and 1 M KOH.

findings highlight the potential applicability of the NiFe-LDH electrocatalysts in real electrolyzer applications, providing a viable and efficient solution for sustainable hydrogen production.

Associated Content in Supporting Information

Figures S1-S7: SEM images for different Ni:Fe ratio, XRD patterns, CV curves, LSV curves for 0 and 25 hours, SEM images of anodic polarization, EDS spectra, LSV curves for 0 and 80. TableS1: EDS analysis.

CRediT authorship contribution statement

Simón G. Quiroz: Writing – original draft, Methodology, Investigation. **Santiago Cartagena:** Writing – review & editing, Supervision, Methodology, Investigation, Conceptualization. **Jorge A. Calderón:** Writing – review & editing, Project administration, Methodology, Funding acquisition, Formal analysis, Conceptualization.

Declaration of competing interest

The authors declare that they have no known competing financial interests or personal relationships that could have appeared to influence the work reported in this paper.

Data availability statement

Data will be made available on request from the interested.

Acknowledgements

The authors thank “Ministerio de Ciencia Tecnología e Innovacion - Minciencias” and “Sistema General de Regalías” for the financial support provided by the project Contract No BPIN 2022000100089.

Supplementary materials

Supplementary material associated with this article can be found, in the online version, at doi:10.1016/j.electacta.2025.146332.

References

[1] T. Nguyen, Z. Abdin, T. Holm, W. Mérida, Grid-connected hydrogen production via large-scale water electrolysis, Energy Convers. Manage 200 (2019) 112108, https://doi.org/10.1016/j.enconman.2019.112108.
[2] J. Chi, H. Yu, Water electrolysis based on renewable energy for hydrogen production, Chin. J. Catal. 39 (2018) 390–394, https://doi.org/10.1016/s1872-2067(17)62949-8.
[3] Green hydrogen cost reduction : scaling up electrolysers to meet the 1.5° C climate goal, IRENA, Abu Dhabi, 2020. https://www.irena.org/publications/2020/Dec/Green-hydrogen-cost-reduction (accessed May 11, 2024).
[4] J. Wang, W. Cui, Q. Liu, Z. Xing, A.M. Asiri, X. Sun, Recent progress in cobalt-based heterogeneous catalysts for electrochemical water splitting, Adv. Mater. 28 (2015) 215–230, https://doi.org/10.1002/adma.201502696.
[5] J. Song, C. Wei, Z.-F. Huang, C. Liu, L. Zeng, X. Wang, Z.J. Xu, A review on fundamentals for designing oxygen evolution electrocatalysts, Chem. Soc. Rev. 49 (2020) 2196–2214, https://doi.org/10.1039/c9cs00607a.
[6] X. Zou, Y. Zhang, Noble metal-free hydrogen evolution catalysts for water splitting, Chem. Soc. Rev. 44 (2015) 5148–5180, https://doi.org/10.1039/c4cs00448e.
[7] J. Lian, Y. Wu, H. Zhang, S. Gu, Z. Zeng, X. Ye, One-step synthesis of amorphous Ni–Fe–P alloy as bifunctional electrocatalyst for overall water splitting in alkaline medium, Int. J. Hydrog. Energy 43 (2018) 12929–12938, https://doi.org/10.1016/j.ijhydene.2018.05.107.
[8] Z. Chen, X. Duan, W. Wei, S. Wang, B.-J. Ni, Iridium-based nanomaterials for electrochemical water splitting, Nano Energy 78 (2020) 105270, https://doi.org/10.1016/j.nanoen.2020.105270.
[9] J. Creus, J. De Tovar, N. Romero, J. García-Antón, K. Philippot, R. Bofill, X. Sala, Ruthenium nanoparticles for catalytic water splitting, ChemSusChem. 12 (2019) 2493–2514, https://doi.org/10.1002/cssc.201900393.
[10] Y. Lee, J. Suntivich, K.J. May, E.E. Perry, Y. Shao-Horn, Synthesis and activities of rutile IrO2 and RuO2 nanoparticles for oxygen evolution in acid and alkaline solutions, J. Phys. Chem. Lett. 3 (2012) 399–404, https://doi.org/10.1021/jz2016507.
[11] Y. Liu, H. Cheng, M. Lyu, S. Fan, Q. Liu, W. Zhang, Y. Zhi, C. Wang, C. Xiao, S. Wei, B. Ye, Y. Xie, Low overpotential in vacancy-rich ultrathin CoSe2 nanosheets for water oxidation, J. Am. Chem. Soc. 136 (2014) 15670–15675, https://doi.org/10.1021/ja5085157.

[12] J. Mohammed-Ibrahim, X. Sun, Recent progress on earth abundant electrocatalysts for hydrogen evolution reaction (HER) in alkaline medium to achieve efficient water splitting – a review, J. Energy Chem. 34 (2019) 111–160, https://doi.org/10.1016/j.jechem.2018.09.016.

[13] M. Ďurovič, J. Hnát, K. Bouzek, Electrocatalysts for the hydrogen evolution reaction in alkaline and neutral media. A comparative review, J. Power. Sources. 493 (2021) 229708, https://doi.org/10.1016/j.jpowsour.2021.229708.

[14] M.-I. Jamesh, X. Sun, Recent progress on earth abundant electrocatalysts for oxygen evolution reaction (OER) in alkaline medium to achieve efficient water splitting – A review, J. Power. Sources. 400 (2018) 31–68, https://doi.org/10.1016/j.jpowsour.2018.07.125.

[15] A.L. Hoang, S. Balakrishnan, A. Hodges, G. Tsekouras, A. Al-Musawi, K. Wagner, C.-Y. Lee, G.F. Swiegers, G.G. Wallace, High-performing catalysts for energy-efficient commercial alkaline water electrolysis, Sustain. Energy Fuels 7 (2023) 31–60, https://doi.org/10.1039/d2se01197b.

[16] F.-Y. Chen, Z.-Y. Wu, Z. Adler, H. Wang, Stability challenges of electrocatalytic oxygen evolution reaction: from mechanistic understanding to reactor design, Joule 5 (2021) 1704–1731, https://doi.org/10.1016/j.joule.2021.05.005.

[17] B. Zhang, Y.H. Lui, H. Ni, S. Hu, Bimetallic (FexNi1−x)2P nanoarrays as exceptionally efficient electrocatalysts for oxygen evolution in alkaline and neutral media, Nano Energy 38 (2017) 553–560, https://doi.org/10.1016/j.nanoen.2017.06.032.

[18] S. Anantharaj, S. Kundu, S. Noda, The Fe Effect": a review unveiling the critical roles of Fe in enhancing OER activity of Ni and Co based catalysts, Nano Energy 80 (2021) 105514, https://doi.org/10.1016/j.nanoen.2020.105514.

[19] M. Tahir, L. Pan, F. Idrees, X. Zhang, L. Wang, J.-J. Zou, Z.L. Wang, Electrocatalytic oxygen evolution reaction for energy conversion and storage: a comprehensive review, Nano Energy 37 (2017) 136–157, https://doi.org/10.1016/j.nanoen.2017.05.022.

[20] L. Han, S. Dong, E. Wang, Transition-metal (Co, Ni, and Fe)-based electrocatalysts for the water oxidation reaction, Adv. Mater. 28 (2016) 9266–9291, https://doi.org/10.1002/adma.201602270.

[21] Y. Qiu, L. Xin, W. Li, Electrocatalytic oxygen evolution over supported small amorphous Ni–Fe nanoparticles in alkaline electrolyte, Langmuir. 30 (2014) 7893–7901, https://doi.org/10.1021/la501246e.

[22] J. Landon, E. Demeter, N. İnoğlu, C. Keturakis, I.E. Wachs, R. Vasić, A.I. Frenkel, J.R. Kitchin, Spectroscopic characterization of mixed Fe–Ni oxide electrocatalysts for the oxygen evolution reaction in alkaline electrolytes, ACS. Catal. 2 (2012) 1793–1801, https://doi.org/10.1021/cs3002644.

[23] R.D.L. Smith, M.S. Prévot, R.D. Fagan, S. Trudel, C.P. Berlinguette, Water oxidation catalysis: electrocatalytic response to metal stoichiometry in amorphous metal oxide films containing iron, cobalt, and nickel, J. Am. Chem. Soc. 135 (2013) 11580–11586, https://doi.org/10.1021/ja403102j.

[24] C. Tang, H.-F. Wang, H.-S. Wang, F. Wei, Q. Zhang, Guest–host modulation of multi-metallic (oxy)hydroxides for superb water oxidation, J. Mater. Chem. Mater. 4 (2016) 3210–3216, https://doi.org/10.1039/c6ta00328a.

[25] Q. Che, Q. Li, Y. Tan, X. Chen, X. Xu, Y. Chen, One-step controllable synthesis of amorphous (Ni-Fe)S /NiFe(OH) hollow microtube/sphere films as superior bifunctional electrocatalysts for quasi-industrial water splitting at large-current-density, Appl. Catal. B 246 (2019) 337–348, https://doi.org/10.1016/j.apcatb.2019.01.082.

[26] Y.-J. Ye, N. Zhang, X.-X. Liu, Amorphous NiFe(oxy)hydroxide nanosheet integrated partially exfoliated graphite foil for high efficiency oxygen evolution reaction, J. Mater. Chem. A Mater. 5 (2017) 24208–24216, https://doi.org/10.1039/c7ta06906e.

[27] Z. Lu, W. Xu, W. Zhu, Q. Yang, X. Lei, J. Liu, Y. Li, X. Sun, X. Duan, Three-dimensional NiFe layered double hydroxide film for high-efficiency oxygen evolution reaction, Chem. Commun 50 (2014) 6479–6482, https://doi.org/10.1039/c4cc01625d.

[28] K. Zhang, R. Zou, Advanced transition metal-based OER electrocatalysts: current status, opportunities, and challenges, Small. 17 (2021), https://doi.org/10.1002/smll.202100129.

[29] L. Lv, Z. Yang, K. Chen, C. Wang, Y. Xiong, 2D Layered double hydroxides for oxygen evolution reaction: from fundamental design to application, Adv. Energy Mater. 9 (2019), https://doi.org/10.1002/aenm.201803358.

[30] J. Zhao, J. Zhang, Z. Li, X. Bu, Recent progress on NiFe-based electrocatalysts for the oxygen evolution reaction, Small. 16 (2020), https://doi.org/10.1002/smll.202003916.

[31] R. Gao, D. Yan, Recent development of Ni/Fe-based micro/nanostructures toward photo/electrochemical water oxidation, Adv. Energy Mater. 10 (2019), https://doi.org/10.1002/aenm.201900954.

[32] M.S. Alnarabiji, S.C.E. Tsang, A.H. Mahadi, Advances in electrode synthesis and fabrication for electrochemical water splitting, Fuel 357 (2024) 129741, https://doi.org/10.1016/j.fuel.2023.129741.

[33] M.B. Kale, R.A. Borse, A. Gomaa Abdelkader Mohamed, Y. Wang, Electrocatalysts by electrodeposition: recent advances, synthesis methods, and applications in energy conversion, Adv. Funct. Mater. 31 (2021) 2101313, https://doi.org/10.1002/adfm.202101313.

[34] J. Kim, H. Kim, G.H. Han, S. Hong, J. Park, J. Bang, S.Y. Kim, S.H. Ahn, Electrodeposition: an efficient method to fabricate self-supported electrodes for electrochemical energy conversion systems, Exploration 2 (2022) 20210077, https://doi.org/10.1002/EXP.20210077.

[35] S.A. Lee, J.W. Yang, S. Choi, H.W. Jang, Nanoscale electrodeposition: dimension control and 3D conformality, Exploration 1 (2021) 20210012, https://doi.org/10.1002/EXP.20210012.

[36] J. Zhao, J.-J. Zhang, Z.-Y. Li, X.-H. Bu, Recent progress on NiFe-based electrocatalysts for the oxygen evolution reaction, Small. 16 (2020) 2003916, https://doi.org/10.1002/smll.202003916.

[37] S. Sun, Y. He, T. Chen, C. Sun, C. Wu, Morphology regulated synthesis of NiFe-layered double hydroxide nanostructures on nickel foam toward efficient oxygen evolution reaction, J. Alloys. Compd. 963 (2023) 171304, https://doi.org/10.1016/j.jallcom.2023.171304.

[38] R. Li, J. Xu, Q. Pan, J. Ba, T. Tang, W. Luo, One-step synthesis of NiFe layered double hydroxide nanosheet array/N-doped graphite foam electrodes for oxygen evolution reactions, ChemistryOpen. 8 (2019) 1027–1032, https://doi.org/10.1002/open.201900190.

[39] K.B. Ibrahim, W.-N. Su, M.-C. Tsai, A.W. Kahsay, S.A. Chala, M.K. Birhanu, J.-F. Lee, B.J. Hwang, Heterostructured composite of NiFe-LDH nanosheets with Ti4O7 for oxygen evolution reaction, Mater. Today Chem. 24 (2022) 100824, https://doi.org/10.1016/j.mtchem.2022.100824.

[40] M. Sreenivasulu, A. Hadrihalli, M.A. Alshehri, N.P. Shetti, Rational designing of nickel–Iron containing layered double hydroxide [NiFe@LDH] electrocatalysts for effective water splitting, Energy Fuels. 38 (2024) 12888–12899, https://doi.org/10.1021/acs.energyfuels.4c01899.

[41] S. Cartagena, J.A. Calderón, High performance of electrochemically modified-polypropylene electrodes for alkaline water splitting, Electrochim. Acta 407 (2022) 139884, https://doi.org/10.1016/j.electacta.2022.139884.

[42] C.C.L. McCrory, S. Jung, J.C. Peters, T.F. Jaramillo, Benchmarking heterogeneous electrocatalysts for the oxygen evolution reaction, J. Am. Chem. Soc. 135 (2013) 16977–16987, https://doi.org/10.1021/ja407115p.

[43] Z.-W. Gao, J.-Y. Liu, X.-M. Chen, X.-L. Zheng, J. Mao, H. Liu, T. Ma, L. Li, W.-C. Wang, X.-W. Du, Engineering NiO/NiFe LDH intersection to bypass scaling relationship for oxygen evolution reaction via dynamic tridimensional adsorption of intermediates, Adv. Mater. 31 (2019) 1804769, https://doi.org/10.1002/adma.201804769.

[44] A.M.P. Sakita, E. Vallés, R. Della Noce, A.V. Benedetti, Novel NiFe/NiFe-LDH composites as competitive catalysts for clean energy purposes, Appl. Surf. Sci. 447 (2018) 107–116, https://doi.org/10.1016/j.apsusc.2018.03.235.

[45] A.A. Kashale, C.-H. Yi, K.-Y. Cheng, J.-S. Guo, Y.-H. Pan, I.-W.P. Chen, Binder-free heterostructured NiFe2O4/NiFe LDH nanosheet composite electrocatalysts for oxygen evolution reactions, ACS. Appl. Energy Mater. 3 (2020) 10831–10840, https://doi.org/10.1021/acsaem.0c01863.

[46] C.X. Guo, C.M. Li, Room temperature-formed iron-doped nickel hydroxide on nickel foam as a 3D electrode for low polarized and high-current-density oxygen evolution, Chem. Commun. 54 (2018) 3262–3265, https://doi.org/10.1039/c8cc00701b.

[47] S. Cartagena, F.E. Bedoya-Lora, J.A. Calderón, Enhancement of anodically treated stainless steel by NiFeP-catalyst electrodeposition as bifunctional electrodes for water electrolysis, J. Electrochem. Soc. 169 (2022) 44501, https://doi.org/10.1149/1945-7111/ac5ff1.

[48] J.O. Silva, S. Cartagena, J.A. Calderón, Novel electrodeposited NiFeP/Zn bifunctional catalytic coating for alkaline water splitting, Electrochim. Acta 451 (2023) 142299, https://doi.org/10.1016/j.electacta.2023.142299.

[49] S. Cartagena, J.A. Calderón, Corrosion of non-noble metal-based catalysts during oxygen evolution reaction under on/off operation, Corros. Sci. 205 (2022) 110437, https://doi.org/10.1016/j.corsci.2022.110437.

[50] N.S. Gultom, H. Abdullah, C.-N. Hsu, D.-H. Kuo, Activating nickel iron layer double hydroxide for alkaline hydrogen evolution reaction and overall water splitting by electrodepositing nickel hydroxide, Chem. Eng. J. 419 (2021) 129608, https://doi.org/10.1016/j.cej.2021.129608.

[51] S. Sirisomboonchai, S. Li, A. Yoshida, X. Li, C. Samart, A. Abudula, G. Guan, Fabrication of NiO microflake@NiFe-LDH nanosheet heterostructure electrocatalysts for oxygen evolution reaction, ACS Sustain. Chem. Eng. 7 (2018) 2327–2334, https://doi.org/10.1021/acssuschemeng.8b05088.

[52] E. Hatami, A. Toghraei, G. Barati Darband, Electrodeposition of Ni–Fe micro/nano urchin-like structure as an efficient electrocatalyst for overall water splitting, Int. J. Hydrog. Energy 46 (2021) 9394–9405, https://doi.org/10.1016/j.ijhydene.2020.12.110.

[53] N. Zech, E.J. Podlaha, D. Landolt, Anomalous codeposition of iron group metals: I. Experimental results, J. Electrochem. Soc. 146 (1999) 2886–2891, https://doi.org/10.1149/1.1392024.

[54] T.-R. Lee, L. Chang, C.-H. Chen, Effect of electrolyte temperature on composition and phase structure of nanocrystalline Fe–Ni alloys prepared by direct current electrodeposition, Surf. Coat. Technol. 207 (2012) 523–528, https://doi.org/10.1016/j.surfcoat.2012.07.069.

[55] M. Matlosz, Competitive adsorption effects in the electrodeposition of iron-nickel alloys, J. Electrochem. Soc. 140 (1993) 2272–2279, https://doi.org/10.1149/1.2220807.

[56] B. Buccheri, F. Ganci, B. Patella, G. Aiello, P. Mandin, R. Inguanta, Ni-Fe alloy nanostructured electrodes for water splitting in alkaline electrolyser, Electrochim. Acta 388 (2021) 138588, https://doi.org/10.1016/j.electacta.2021.138588.

[57] H. Dahms, I.M. Croll, The anomalous codeposition of iron-nickel alloys, J. Electrochem. Soc. 112 (1965) 771, https://doi.org/10.1149/1.2423692.

[58] S. Zhang, J. Yu, Z. Liu, Y. Yin, C. Qiao, Numerical and experimental investigation of the effect of current density on the anomalous codeposition of ternary Fe-Co-Ni alloy coatings, Mater. (Basel) 15 (2022) 6141, https://doi.org/10.3390/ma15176141.

[59] H. Nakano, M. Matsuno, S. Oue, M. Yano, S. Kobayashi, H. Fukushima, Mechanism of anomalous type electrodeposition of Fe-Ni alloys from sulfate solutions, Nippon Kinzoku Gakkaishi/J. Jpn. Inst. Met. 69 (2005) 548–554, https://doi.org/10.2320/jinstmet.69.548.

[60] D. Guo, H. Xia, X. Guo, L. Wen, T. Wang, X. Li, Z. Sun, Synthesis bifunctional catalysts with amorphous NiFe-LDH/crystalline CoMo bimetallic phosphide heterojunction by electrodeposition for efficient water splitting, Int. J. Hydrog. Energy 79 (2024) 73–85, https://doi.org/10.1016/j.ijhydene.2024.06.426.
[61] J. Liu, J. Zhou, S. Liu, G. Chen, W. Wu, Y. li, P. Jin, C. Xu, Amorphous NiFe-layered double hydroxides nanosheets for oxygen evolution reaction, Electrochim. Acta 356 (2020) 136827, https://doi.org/10.1016/j.electacta.2020.136827.
[62] J. Nie, M. Hong, X. Zhang, J. Huang, Q. Meng, C. Du, J. Chen, 3D amorphous NiFe LDH nanosheets electrodeposited on in situ grown NiCoP@NC on nickel foam for remarkably enhanced OER electrocatalytic performance, Dalton Trans. 49 (2020) 4896–4903, https://doi.org/10.1039/C9DT04888J.
[63] X. Chen, X. Yu, C. Yang, G. Wang, Enhancing OER and overall water splitting performance of amorphous NiFe LDH grown on Ni foam with the needle-like NiCoP transition layer, J. Solid. State Chem. 333 (2024) 124649, https://doi.org/10.1016/j.jssc.2024.124649.
[64] Y. Li, S. Guo, T. Jin, Y. Wang, F. Cheng, L. Jiao, Promoted synergy in core-branch CoP@NiFe–OH nanohybrids for efficient electrochemical-/photovoltage-driven overall water splitting, Nano Energy 63 (2019) 103821, https://doi.org/10.1016/j.nanoen.2019.06.017.
[65] H. Liang, A.N. Gandi, C. Xia, M.N. Hedhili, D.H. Anjum, U. Schwingenschlögl, H. N. Alshareef, Amorphous NiFe-OH/NiFeP electrocatalyst fabricated at low temperature for water oxidation applications, ACS. Energy Lett. 2 (2017) 1035–1042, https://doi.org/10.1021/acsenergylett.7b00206.
[66] H. Li, L. Zhang, S. Wang, J. Yu, Accelerated oxygen evolution kinetics on NiFeAl-layered double hydroxide electrocatalysts with defect sites prepared by electrodeposition, Int. J. Hydrog. Energy 44 (2019) 28556–28565, https://doi.org/10.1016/j.ijhydene.2019.09.155.
[67] Y. Feng, R. Ma, M. Wang, J. Wang, T. Sun, L. Hu, J. Zhu, Y. Tang, J. Wang, Crystallinity effect of NiFe LDH on the growth of Pt nanoparticles and hydrogen evolution performance, J. Phys. Chem. Lett. 12 (2021) 7221–7228, https://doi.org/10.1021/acs.jpclett.1c02095.
[68] L. Yu, H. Zhou, J. Sun, I.K. Mishra, D. Luo, F. Yu, Y. Yu, S. Chen, Z. Ren, Amorphous NiFe layered double hydroxide nanosheets decorated on 3D nickel phosphide nanoarrays: a hierarchical core–shell electrocatalyst for efficient oxygen evolution, J. Mater. Chem. A 6 (2018) 13619–13623, https://doi.org/10.1039/C8TA02967A.
[69] X. Lu, C. Zhao, Electrodeposition of hierarchically structured three-dimensional nickel–iron electrodes for efficient oxygen evolution at high current densities, Nat. Commun. 6 (2015), https://doi.org/10.1038/ncomms7616.
[70] A. Ahlawat, V.G. Sathe, Raman study of NiFe2O4 nanoparticles, bulk and films: effect of laser power, J. Raman Spectrosc. 42 (2010) 1087–1094, https://doi.org/10.1002/jrs.2791.
[71] Z. Wu, Z. Zou, J. Huang, F. Gao, NiFe2O4 Nanoparticles/NiFe layered double-hydroxide nanosheet heterostructure array for efficient overall water splitting at large current densities, ACS Appl. Mater. Interfaces 10 (2018) 26283–26292, https://doi.org/10.1021/acsami.8b07835.
[72] G. Liu, K. Wang, X. Gao, D. He, J. Li, Fabrication of mesoporous NiFe2O4 nanorods as efficient oxygen evolution catalyst for water splitting, Electrochim. Acta 211 (2016) 871–878, https://doi.org/10.1016/j.electacta.2016.06.113.
[73] H. Lei, L. Ma, Q. Wan, S. Tan, B. Yang, Z. Wang, W. Mai, H.J. Fan, Promoting surface reconstruction of NiFe layered double hydroxide for enhanced oxygen evolution, Adv. Energy Mater. 12 (2022), https://doi.org/10.1002/aenm.202202522.
[74] S. Lee, K. Banjac, M. Lingenfelder, X. Hu, Oxygen isotope labeling experiments reveal different reaction sites for the Oxygen evolution reaction on nickel and nickel iron oxides, Angew. Chem. 131 (2019) 10401–10405, https://doi.org/10.1002/ange.201903200.
[75] L. Yan, Y. Ren, J. Shen, H. Wang, J. Ning, Y. Zhong, Y. Hu, Visible-light-driven electrocatalytic oxygen evolution reaction: NiFe2O4/NiFe–Layered double hydroxide Z-scheme heteronanosheet as a model, Energy Technol. 8 (2020), https://doi.org/10.1002/ente.202000607.
[76] Y. Luo, Y. Wu, D. Wu, C. Huang, D. Xiao, H. Chen, S. Zheng, P.K. Chu, NiFe-layered double hydroxide synchronously activated by heterojunctions and vacancies for the oxygen evolution reaction, ACS Appl. Mater. Interfaces 12 (2020) 42850–42858, https://doi.org/10.1021/acsami.0c11847.
[77] D. Bokov, A. Turki Jalil, S. Chupradit, W. Suksatan, M. Javed Ansari, I. H. Shewael, G.H. Valiev, E. Kianfar, Nanomaterial by sol-gel method: synthesis and application, Adv. Mater. Sci. Eng. 2021 (2021) 5102014, https://doi.org/10.1155/2021/5102014.
[78] F. Majid, J. Rauf, S. Ata, I. Bibi, A. Malik, S.M. Ibrahim, A. Ali, M. Iqbal, Synthesis and characterization of NiFe2O4 ferrite: sol–gel and hydrothermal synthesis routes effect on magnetic, structural and dielectric characteristics, Mater. Chem. Phys. 258 (2021) 123888, https://doi.org/10.1016/j.matchemphys.2020.123888.
[79] H. Zhong, T. Liu, S. Zhang, D. Li, P. Tang, N. Alonso-Vante, Y. Feng, Template-free synthesis of three-dimensional NiFe-LDH hollow microsphere with enhanced OER performance in alkaline media, J. Energy Chem. 33 (2019) 130–137, https://doi.org/10.1016/j.jechem.2018.09.005.
[80] M. Sreenivasulu, N.K.V. Hiremath, M.A. Alshehri, N.P. Shetti, A green solvent-free approach synthesis for rational designing of a NiFe-layered double hydroxide [NiFe-LDH] electrocatalyst for hydrogen generation, Energy Fuels. 38 (2024) 20791–20806, https://doi.org/10.1021/acs.energyfuels.4c03780.
[81] Y. Wang, S. Tao, H. Lin, G. Wang, K. Zhao, R. Cai, K. Tao, C. Zhang, M. Sun, J. Hu, B. Huang, S. Yang, Atomically targeting NiFe LDH to create multivacancies for OER catalysis with a small organic anchor, Nano Energy 81 (2021) 105606, https://doi.org/10.1016/j.nanoen.2020.105606.
[82] Y. Zhang, C. Zhang, Y. Mei, T. Le, H. Shao, H. Jiang, Y. Feng, J. Hu, NiFe layered double hydroxide as an efficient bifunctional catalyst for electrosynthesis of hydrogen peroxide and oxygen, Int. J. Hydrog. Energy 47 (2022) 36831–36842, https://doi.org/10.1016/j.ijhydene.2022.08.250.
[83] F. Chen, S. Zhang, J. Li, A. Kan, M. Yang, J. Zhao, G. Deng, Precursor-mediated synthesis of interconnected ultrathin NiFe-layered double hydroxides nanosheets for efficient oxygen evolution electrocatalysis, Mater. Lett. 309 (2022) 131470, https://doi.org/10.1016/j.matlet.2021.131470.
[84] Y. Zhou, Q. Guo, J. Luo, X. Wang, F. Sun, C. Wang, S. Wang, J. Zhang, The influence of increased content of Ni(III) in NiFe LDH via Zn doping on electrochemical catalytic oxygen evolution reaction, Int. J. Hydrog. Energy 48 (2023) 4984–4993, https://doi.org/10.1016/j.ijhydene.2022.11.075.
[85] Y. Yang, S. Wei, Y. Li, D. Guo, H. Liu, L. Liu, Effect of cobalt doping-regulated crystallinity in nickel-iron layered double hydroxide catalyzing oxygen evolution, Appl. Catal. B 314 (2022) 121491, https://doi.org/10.1016/j.apcatb.2022.121491.
[86] H. Xu, W.-D. Zhang, J. Liu, Y. Yao, X. Yan, Z.-G. Gu, Intercalation-induced partial exfoliation of NiFe LDHs with abundant active edge sites for highly enhanced oxygen evolution reaction, J. Colloid. Interface Sci. 607 (2022) 1353–1361, https://doi.org/10.1016/j.jcis.2021.09.105.
[87] C. He, X. Kong, M. Jiang, X. Lei, Metal Ni-decorated Fe 3 O 4 nanoparticles: a new and efficient electrocatalyst for oxygen evolution reaction, Mater. Lett. 222 (2018) 138–141, https://doi.org/10.1016/j.matlet.2018.03.142.
[88] Y. Han, J. Wu, L. Tang, X. An, X. Yang, T. Li, Q. Wang, X. Wu, Self-adaption of Zn introduced Ni-Fe layered double hydroxide for efficient and durable oxygen evolution reaction electrocatalysis, Appl. Surf. Sci. 610 (2023) 155288, https://doi.org/10.1016/j.apsusc.2022.155288.
[89] X. Lyu, Y. Zhang, X. Wang, H. Chen, S. Li, W. Zhang, Y. Hu, F. Li, D. Li, D. Yang, Electronic structure regulation of nickel-iron layered double hydroxides by tuning ternary component for overall water splitting, Mater. Today Sustain. 21 (2023) 100295, https://doi.org/10.1016/j.mtsust.2022.100295.
[90] C. Qiao, Z. Usman, T. Cao, S. Rafai, Z. Wang, Y. Zhu, C. Cao, J. Zhang, High-valence Ni and Fe sites on sulfated NiFe-LDH nanosheets to enhance O-O coupling for water oxidation, Chem. Eng. J. 426 (2021) 130873, https://doi.org/10.1016/j.cej.2021.130873.
[91] Q. Chen, Z. Kang, S. Luo, J. Li, P. Deng, C. Wang, Y. Hua, S. Zhong, X. Tian, Boosting NiFe-LDH by ruthenium dioxide for effective overall water splitting, Int. J. Hydrog. Energy 48 (2023) 8888–8897, https://doi.org/10.1016/j.ijhydene.2022.11.295.
[92] Q. Wen, S. Wang, R. Wang, D. Huang, J. Fang, Y. Liu, T. Zhai, Nanopore-rich NiFe LDH targets the formation of the high-valent nickel for enhanced oxygen evolution reaction, Nano Res. 16 (2022) 2286–2293, https://doi.org/10.1007/s12274-022-5163-z.
[93] S. He, R. Yue, W. Liu, J. Ding, X. Zhu, N. Liu, R. Guo, Z. Mo, Nano-NiFe LDH assembled on CNTs by electrostatic action as an efficient and durable electrocatalyst for oxygen evolution, J. Electroanal. Chem. 946 (2023) 117718, https://doi.org/10.1016/j.jelechem.2023.117718.
[94] A. Alobaid, C. Wang, R.A. Adomaitis, Mechanism and kinetics of HER and OER on NiFe LDH films in an Alkaline electrolyte, J. Electrochem. Soc. 165 (2018) J3395–J3404, https://doi.org/10.1149/2.0481815jes.
[95] L. Negahdar, F. Zeng, S. Palkovits, C. Broicher, R. Palkovits, Mechanistic aspects of the electrocatalytic oxygen evolution reaction over Ni−Co oxides, ChemElectroChem. 6 (2019) 5588–5595, https://doi.org/10.1002/celc.201901265.
[96] H. Yang, C. Wang, Y. Zhang, Q. Wang, Green synthesis of NiFe LDH/Ni foam at room temperature for highly efficient electrocatalytic oxygen evolution reaction, Sci. China Mater. 62 (2018) 681–689, https://doi.org/10.1007/s40843-018-9356-1.
[97] S. Liu, H. Zhang, E. Hu, T. Zhu, C. Zhou, Y. Huang, M. Ling, X. Gao, Z. Lin, Boosting oxygen evolution activity of NiFe-LDH using oxygen vacancies and morphological engineering, J. Mater. Chem. A Mater. 9 (2021) 23697–23702, https://doi.org/10.1039/d1ta06263h.
[98] G. Li, L. Anderson, Y. Chen, M. Pan, P.-Y. Abel Chuang, New insights into evaluating catalyst activity and stability for oxygen evolution reactions in alkaline media, Sustain. Energy Fuels 2 (2018) 237–251, https://doi.org/10.1039/c7se00337d.
[99] L. Sondermann, W. Jiang, M. Shviro, A. Spieß, D. Woschko, L. Rademacher, C. Janiak, Nickel-based metal-organic frameworks as electrocatalysts for the oxygen evolution reaction (OER), Molecules. 27 (2022) 1241, https://doi.org/10.3390/molecules27041241.
[100] T.H.Y. Beglau, M.N.A. Fetzer, I. Boldog, T. Heinen, M. Suta, C. Janiak, G. Yücesan, Exceptionally stable and super-efficient electrocatalysts derived from semiconducting metal phosphonate frameworks, Chem. – Eur. J. 30 (2023), https://doi.org/10.1002/chem.202302765.
[101] B. Chen, Z. Zhang, S. Kim, S. Lee, J. Lee, W. Kim, K. Yong, Ostwald ripening driven exfoliation to ultrathin layered double hydroxides nanosheets for enhanced oxygen evolution reaction, ACS Appl. Mater. Interfaces 10 (2018) 44518–44526, https://doi.org/10.1021/acsami.8b16962.
[102] C.C.L. McCrory, S. Jung, I.M. Ferrer, S.M. Chatman, J.C. Peters, T.F. Jaramillo, Benchmarking hydrogen evolving reaction and oxygen evolving reaction electrocatalysts for solar water splitting devices, J. Am. Chem. Soc. 137 (2015) 4347–4357, https://doi.org/10.1021/ja510442p.
[103] J. Lian, Y. Wu, J. Sun, High current density electrodeposition of NiFe/nickel foam as a bifunctional electrocatalyst for overall water splitting in alkaline electrolyte,

J. Mater. Sci. 55 (2020) 15140–15151, https://doi.org/10.1007/s10853-020-05080-w.
[104] Y. Gu, D.-H. Park, M.-H. Kim, J.-H. Byeon, D.-M. Lim, S.-H. Park, J.-H. Kim, J.-S. Jang, K.-W. Park, NiFe layered double hydroxides synthesized based on solvent properties as anode catalysts for enhanced oxygen evolution reaction, Chem. Eng. J. 480 (2024) 147789, https://doi.org/10.1016/j.cej.2023.147789.
[105] W. Bao, C. Yang, T. Ai, J. Zhang, L. Zhou, Y. li, X. Wei, X. Zou, Y. Wang, Modulating interfacial charge distribution of NiSe nanoarrays with NiFe-LDH nanosheets for boosting oxygen evolution reaction, Fuel 332 (2023) 126227, https://doi.org/10.1016/j.fuel.2022.126227.
[106] S.S. Jeon, P.W. Kang, M. Klingenhof, H. Lee, F. Dionigi, P. Strasser, Active surface area and intrinsic catalytic oxygen evolution reactivity of NiFe LDH at reactive electrode potentials using capacitances, ACS. Catal. 13 (2023) 1186–1196, https://doi.org/10.1021/acscatal.2c04452.
[107] R.L. Doyle, M.E.G. Lyons, An electrochemical impedance study of the oxygen evolution reaction at hydrous iron oxide in base, Phys. Chem. Chem. Phys. 15 (2013) 5224, https://doi.org/10.1039/c3cp43464h.
[108] J. Chen, F. Zheng, S.-J. Zhang, A. Fisher, Y. Zhou, Z. Wang, Y. Li, B.-B. Xu, J.-T. Li, S.-G. Sun, Interfacial interaction between FeOOH and Ni–Fe LDH to modulate the local electronic structure for enhanced OER electrocatalysis, ACS. Catal. 8 (2018) 11342–11351, https://doi.org/10.1021/acscatal.8b03489.
[109] F. Dionigi, P. Strasser, NiFe-based (Oxy)hydroxide catalysts for oxygen evolution reaction in non-acidic electrolytes, Adv. Energy Mater. 6 (2016) 1600621, https://doi.org/10.1002/aenm.201600621.
[110] B.J. Trześniewski, O. Diaz-Morales, D.A. Vermaas, A. Longo, W. Bras, M.T. M. Koper, W.A. Smith, In situ observation of active oxygen species in Fe-containing Ni-based oxygen evolution catalysts: the effect of pH on electrochemical activity, J. Am. Chem. Soc. 137 (2015) 15112–15121, https://doi.org/10.1021/jacs.5b06814.
[111] M.W. Louie, A.T. Bell, An investigation of thin-film Ni–Fe oxide catalysts for the electrochemical evolution of oxygen, J. Am. Chem. Soc. 135 (2013) 12329–12337, https://doi.org/10.1021/ja405351s.
[112] R.J. Gilliam, J.W. Graydon, D.W. Kirk, S.J. Thorpe, A review of specific conductivities of potassium hydroxide solutions for various concentrations and temperatures, Int. J. Hydrog. Energy 32 (2007) 359–364, https://doi.org/10.1016/j.ijhydene.2006.10.062.
[113] J. Brauns, T. Turek, Alkaline water electrolysis powered by renewable energy: a review, Processes 8 (2020), https://doi.org/10.3390/pr8020248.
[114] J.A.D. del Rosario, G. Li, M.F.M. Labata, J.D. Ocon, P.-Y.A. Chuang, Unravelling the roles of alkali-metal cations for the enhanced oxygen evolution reaction in alkaline media, Appl. Catal. B 288 (2021) 119981, https://doi.org/10.1016/j.apcatb.2021.119981.
[115] J. Suntivich, E.E. Perry, H.A. Gasteiger, Y. Shao-Horn, The influence of the cation on the oxygen reduction and evolution activities of oxide surfaces in alkaline electrolyte, Electrocatalysis 4 (2012) 49–55, https://doi.org/10.1007/s12678-012-0118-x.
[116] G.-F. Li, M. Divinagracia, M.F. Labata, J.D. Ocon, P.-Y. Abel Chuang, Electrolyte-dependent oxygen evolution reactions in alkaline Media: electrical double layer and interfacial interactions, ACS. Appl. Mater. Interfaces. 11 (2019) 33748–33758, https://doi.org/10.1021/acsami.9b06889.
[117] H. Khani, A.R. Puente Santiago, T. He, An interfacial view of cation effects on electrocatalysis systems, Angew. Chem. 135 (2023), https://doi.org/10.1002/ange.202306103.